ACS APPLIED MATERIALS & INTERFACES

Research Article

www.acsami.org

Mercaptoundecanoic Acid Capped Palladium Nanoparticles in a SAPO 34 Membrane: A Solution for Enhancement of H_2/CO_2 Separation Efficiency

Jugal Kishore Das and Nandini Das*

Ceramic Membrane Division, Central Glass and Ceramic Research Institute, Council of Scientific and Industrial Research, 196 Raja S. C. Mullick Road, Jadavpur, Kolkata, West Bengal 700 032, India

Supporting Information

ABSTRACT: In this work, the high quality Pd/SAPO 34 membranes were grown on the support using a secondary (seeded) growth hydrothermal technique followed by insertion of 11-mercaptoundecanoic acid capped palladium (MUA-Pd) nanoparticles (NPs) to the membrane surface. For this, first, the indigenous low cost clay−alumina support was treated with poly diallyldimethylammonium chloride (PolyDADMAC) polymer, and subsequently, a seed layer of SAPO 34 crystals was deposited homogeneously in a regular orientation. Since PolyDADMAC is a high charge density cationic polymer, it assisted in reversing the charge of the support surface and produced an attractive electrostatic interaction between the support and zeolite crystals. This may facilitate the zeolite grain orientation in the synthesized membrane layer. Here, the Pd NPs were deposited in the membrane matrix by a simple dip-coating method. After thermal treatment of the Pd/SAPO 34 membrane, the defects were formed because of the removal of the structure-directing agent (SDA) from the zeolite pores but the presence of Pd NPs, which were entrapped inside the nonzeolitic pores and clogged the defects of the membrane. Field emission scanning electron microscopy (FESEM) and elemental mapping of the membrane cross-section confirmed that most of the Pd NPs were deposited at the interface of the membrane and the support layer which may increase the membrane efficiency, i.e., separation factor, as well as permeability of H_2 through the membrane. As the membrane structure was associated with the oriented crystal, the pores were more aligned and permeation adequacy of H_2 through the membrane enhanced. These membranes have a relative hydrogen permeance of 14.8×10^{-7} mol·m^{-2}·s^{-1}·Pa^{-1}. The selectivity of H_2/CO_2 based on single gas permeation was 10.6, but for the mixture gas (H_2/CO_2 55:45), the H_2/CO_2 mixture separation factor increased up to 20.8 at room temperature. It is anticipated that this technique may be useful for making a defect free membrane and also a hydrogen selective Pd loaded membrane with lower cost (as the quantity of Pd is low) which can be utilized for a "clean energy" related application.

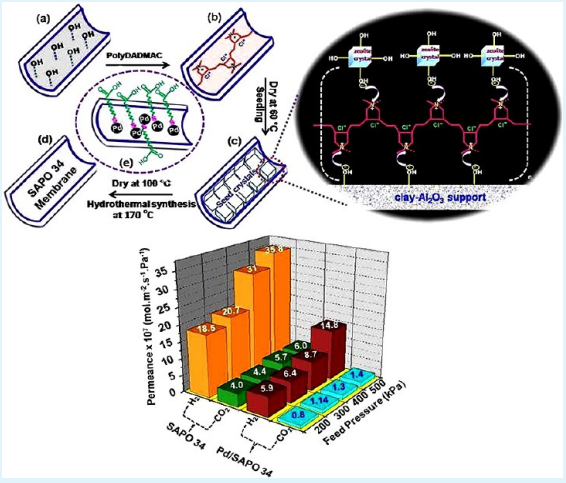

KEYWORDS: *Pd/SAPO 34 membrane, secondary growth, nonzeolitic pore, hydrogen separation, selectivity*

1. INTRODUCTION

Hydrogen is often referred to as "clean energy" as it is nonpolluting and ultimately by oxidation it forms only water.[1] However, the production of hydrogen from hydrocarbons, yields CO_2, a green house gas. Thus, to acquire high purity hydrogen from either syngas or the products of the water−gas shift reaction,[2] separation of H_2 from either CO or CO_2 is necessary. Membrane technology has been the center of research for such hydrogen separation because of its energy saving potential. Zeolites are routinely used in heterogeneous catalytic reactions, ion exchanges, sensors, corrosion protection coatings, and microelectronics devices, and conspicuously, they have been utilized for gas separation applications due to their potential advantages of well-defined pore structure, adsorption properties, and high thermal and chemical stability.[3,4] Among different types of zeolite,[5−10] SAPO 34 has been successfully employed in gas separation,[11] catalytic application,[12] hydrocarbons transformation,[13] etc. It is a microporous crystalline silicoaluminophosphate molecular sieve with a chabazite (CHA) type framework that consists of double six-ring prisms (D6Rs) arranged in layers linked by tilted four-membered rings (4MRs) having 8-ring apertures with a pore diameter of 3.8 A^0 (Figure 1) that permits access to a 3-D channel and cage system.[14] Such geometry allows molecules with small kinetic diameters to easily diffuse through the crystal structure, and mostly, these are more preferred for gas separation

Received: July 11, 2014
Accepted: October 29, 2014
Published: October 29, 2014

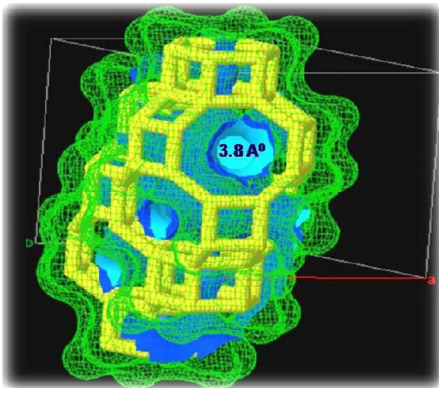

Figure 1. Chabazite type (CHA) framework consists of double six-ring prisms (D6Rs) arranged in layers linked by tilted four-membered rings (4MRs) having 8-ring apertures with a pore diameter of 3.8 A^0. A three-dimensional view (According to the database of zeolite structures available from the International Zeolite Association: http://www.iza-structure.org/databases/).

application.[15−20] In the polycrystalline zeolite membrane, the existence of defects is one of the major hurdles for large scale application.[21−23] The cracks or pinholes usually correspond to macrodefects, while mesodefects and microdefects are intercrystalline boundaries that are primarily formed by imperfect intergrowth between the zeolite crystal grains during hydrothermal synthesis. Furthermore, the defects are generally formed during the thermal treatment of the membrane for the removal of structure-directing agent (SDA) from zeolitic pores.[24]

Hence, to take advantage of the molecular-sieving and preferential adsorption properties of zeolite pores, both defect number and size must be minimized to increase the performance of the membrane. Thus, the elimination of possible defects in polycrystalline zeolite membranes is indispensable and really a big challenge for their practical application. Until now, much effort has been made toward eliminating defects in polycrystalline zeolite membranes by postsynthetic treatments like hydrocarbon impregnation and coking,[25,26] surface coating,[27−29] chemical vapor deposition (CVD),[30,31] chemical liquid deposition (CLD),[23] etc. All these methods have some advantages and disadvantages. These methods were successful and achieved higher selectivity, but the flux was significantly reduced due to the blockage of zeolite pores. Besides, all the methods were performed at very high temperatures, and the increased selectivity was achieved at the cost of a serious flux decrease. Anthonis et al.[32] reported a new technique to reduce the defects in the zeolite membrane by fabricating a top layer of refractory material. In this case, the refractory layer could occlude the defects present in the zeolite layer with no effect on the zeolite pores. However, during calcination at high temperatures and repeated operation cycles, new cracks could be formed. Previously, an attempt was also taken to block the nonzeolitic pores by chemical vapor deposition (CVD) of Pd nanoparticles (NPs) over the zeolite membrane.[33] Recently, Zhang and co-workers fabricated Pd/Si-MFI membranes by depositing Pd nanoparticles onto the membranes via chemical fluid deposition in supercritical CO_2 to plug the defects present within the matrix,[34] but this technique is not cost-effective because it follows the CVD and CFT route for nanoparticle deposition.

To solve the problem mentioned above, here, an attempt has been made to demonstrate an easy method for the fabrication of Pd loaded SAPO 34 zeolite membrane on the surface modified low-cost clay−alumina tubular support for separation of H_2/CO_2 in order to produce clean hydrogen. It is well-known that the secondary (seeded) growth method has been revealed to be an influential one and provoked great research interests in zeolite membranes synthesis.[35] However, some disadvantages are also observed with this technique. Usually, the main problem associated with zeolite coating synthesis onto the support is crack formation. As the support layer and zeolite seed crystals bear a negative surface charge,[36] electrostatic repulsion due to the same surface charges inhibits the adsorption of zeolite particles onto the support surface which may lead to inhomogeneous growth of the membrane layer. Hence, a positive support surface is expected to promote zeolite particle sorption, and as a result, the formation of a crack may be reduced by applying an intermediate layer between the support surface and seed layer.[37,38]

In this protocol, the use of cationic polymer poly diallyldimethylammonium chloride (PolyDADMAC) allowed the charge of the support surface to be reversed; a positively charged substrate was obtained, and an attractive electrostatic interaction between the support and the zeolite seed crystals was produced.[39,40] This may facilitate the formation of a homogeneous and oriented zeolite layer. After successful synthesis of the SAPO 34 membrane, it was targeted for the Pd NPs insertion to reduce the cracks and defects which were formed during the calcinations process as shown schematically in Scheme 1. As a result, the hydrogen gas permeability as well

Scheme 1. Schematic Outlook of 11-Mercaptoundecanoic Acid Capped Palladium Nanoparticles (MUA-Pd NPs) Loaded in the SAPO 34 Membrane Layer[a]

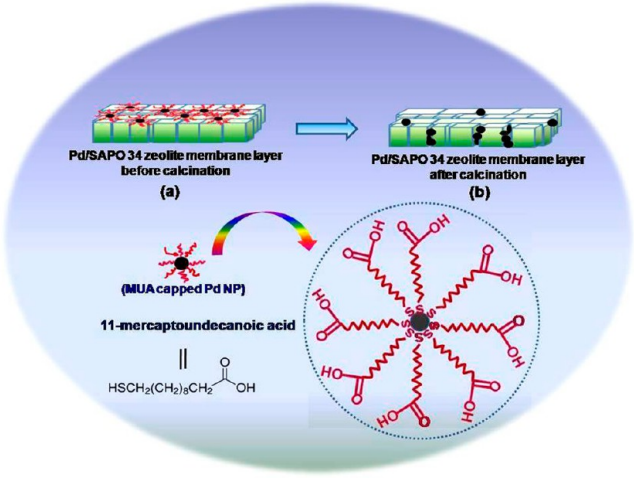

[a](a) Before calcinations, and (b) after calcinations.

as H_2/CO_2 separation efficiency can be improved simultaneously. Besides the above-mentioned possibility, the insertion of Pd NPs on the porous support may be of great interest and useful in chemical industry.[41]

Usually, metal nanoparticles with controlled particle size and structures may be prepared using synthetic methods involving solution-based colloidal chemistry.[42] In this procedure, the presynthesized Pd NPs were stabilized with certain a surfactant and capping agent and dispersed throughout the membrane

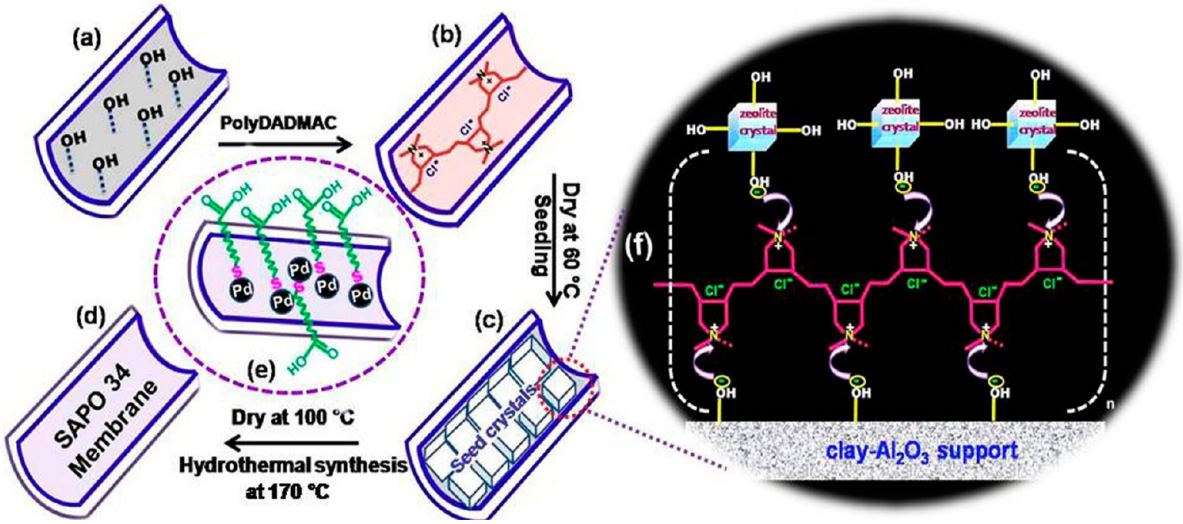

Figure 2. Schematic illustration of different steps involved during the synthesis of the SAPO 34 membrane starting from (a) bare substrate, (b) PolyDADMAC modified layer, (c) seed monolayer onto the modified support, (d) synthesized membrane by the secondary growth hydrothermal process, (e) the membrane layer decorated with MUA-capped Pd NPs, and (f) the corresponding binding mechanism between support and zeolite crystals via the PolyDADMAC intermediate layer.

surface by simple dip coating techniques. Here, the presynthesized Pd NPs size was approximately 4−5 nm. Previously, small thiol-protected Pd NPs have been prepared with 11-mercaptoundecanoic acid by a simple scale-up synthesis route.[43] According to the literature, the use of capped Pd, having 2−5 nm particle size, usually minimizes the costs.[44] As the hydrodynamic radius of NPs was much larger than the cavity size of the SAPO 34 zeolite, the NPs cannot occupy the cavities but instead were surrounded by the membrane surface as well as entrapped inside the nonzeolitic pores after the calcinations process as shown schematically (Scheme1). The detailed explanations for repairing the nonzeolitic pores by the NPs insertion and developing a "reduced defect" membrane for hydrogen gas separation from CO_2 has been described in the Results and Discussion. For better understanding, the gas permeation studies were carried out by using the Pd/SAPO 34 membranes and SAPO membrane without Pd loading. It is an easy route to fabricate the Pd/SAPO 34 membrane on a low-cost clay−alumina support and may be a possible solution for synthesizing an almost defect free membrane for gas separation application. Our approach toward the deposition of Pd NPs in zeolite membrane is very simple and cost-effective which may help for catalytic membrane synthesis in the future.

2. EXPERIMENTAL SECTION

Materials and Membrane Preparation. All chemicals were used as received. Ludox AS-40 colloidal silica (SiO_2, 40 wt %), phosphoric acid (H_3PO_4, 85 wt %), 11-mercaptoundecanoic acid (MUA, 95%), sodium borohydride ($NaBH_4$), potassium tetrachloropalladate(II) (K_2PdCl_4), and poly diallyldimethylammonium chloride solution (PolyDADMAC, 20% in water) were purchased from Sigma-Aldrich. Boehmite powder as an alumina source was purchased from SASOL, Germany while morpholine and acetone were purchased from Merck, India. Water was purified using a Millipore Milli-Q system (18.2 MΩ·cm). Hydrogen (99.99%), carbon dioxide (99.99%), nitrogen (99.99%), and oxygen (99.99%) were obtained from BOC India Ltd. An indigenous clay−alumina tube of 10 mm diameter, 3 mm thickness, and 60 mm length was used as support for synthesis of the membrane.

At the first step, SAPO-34 seeds were prepared by a hydrothermal process from a saturated gel having the molecular composition $Al_2O_3/SiO_2/P_2O_5/H_2O$ 1:0.3:1:66 and morpholin as a structure-directing agent (SDA). The detailed synthesis scheme was discussed in our previous report.[45] The size range of seed crystals was ∼2−3 μm.

Prior to seeding, the support was cleaned with acetone in an ultrasonic cleaner (Vibracell, USA) for 10−15 min to remove the dust particles and oily matter. The outer surface of the support tubes was wrapped with Teflon tape, so that the zeolite layer was formed inside the tube. Subsequently, the support was modified by cationic polymer PolyDADMAC (0.5 wt % in 20 mL of H_2O) and dried at 60 °C for 30 min leading to DADMAC polycations adsorbed on the clay−alumina support surface. The treated support substrate was dipped in a 3% SAPO 34 zeolite seed suspension in deionized water three times for a duration of 20 s. After the dipping procedure, the seeded supports were dried at 100 °C for 24 h. Afterward, the seeded substrates were placed vertically in an autoclave filled with a reaction mixture of the same composition as that employed for SAPO-34 seed synthesis. Then, SAPO-34 membranes were prepared inside the tubular porous support by the secondary-seeded growth hydrothermal technique at 170 °C for 120 h. After synthesis, the zeolite coated membrane was washed thoroughly with deionized water several times and then dried in air at 100 °C overnight.

Insertion of Pd NPs onto SAPO 34 Membrane. First, water-soluble mercaptoundecanoic acid capped palladium nanoparticles (MUA-Pd) were synthesized by adding the reducing agent $NaBH_4$ at a slow rate under ambient atmosphere. In a typical synthesis, 25.9 mg of K_2PdCl_4 was first dissolved in 5 mL of water, and then, 20 mL of acetone was added. To the red solution, phosphoric acid (61 mol vs Pd) and 11-mercaptoundecanoic acid (MUA, 0.6 mol vs Pd) was added and stirred for 30 min. After the addition of MUA, the color of the solution changed from red to orange. The temperature was adjusted to 0 °C by means of an ice bath, and then, a freshly prepared aqueous solution (1−2 mL) of $NaBH_4$ (10 mol vs Pd) was added dropwise, until the solution turned black. Pd NPs were precipitated out from the solution after addition of $NaBH_4$ and washed with an acetone/methanol mixture followed by sonication and centrifugation (4500 rpm, 10 min) after each washing cycle. Finally, water-soluble Pd NPs were dispersed by Milli-Q water to prepare 1% and 3% (by wt %) solution and deposited on the SAPO 34 zeolite membrane surface by a simple dip-coating technique. After loading of Pd NPs on the zeolite membrane layer, samples were dried at 100 °C for 1 h and calcined at 550 °C for 5 h under an inert atmosphere. The calcination heating and cooling rates were 1.5 and 1 °C min^{-1}, respectively.

Characterization. The size of the Pd NPs and the implicated Pd particles in the membrane surface were observed through transmission

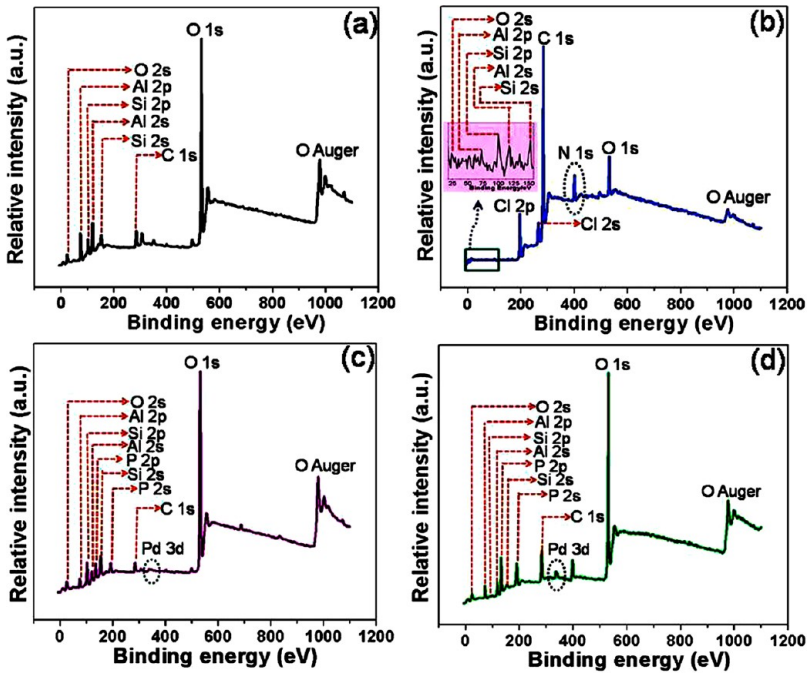

Figure 3. XPS pattern of (a) nonmodified clay–alumina support, (b) PolyDADMAC modified support, (c) Pd/SAPO 34 membrane, and (d) Pd/SAPO 34 membrane calcined under an inert atmosphere.

electron microscopy (TEM). TEM and HRTEM (high resolution transmission electron microscopy) was performed using a Tecnai G2 30ST (FEI company, USA) operating at 300 kV. TEM samples were prepared by drop casting of diluted MUA-capped Pd NPs and scratching off the coatings of the Pd/SAPO 34 membrane layer onto the carbon-coated Cu grids. The crystalline pattern of the SAPO 34 membrane and Pd/SAPO 34 membrane was demonstrated by X-ray diffraction (Philips 1710 diffractometer using Cu Kα radiation (α = 1.541 A°)). The microstructure, elemental mapping with EDAX, and cross sectional line scanning of the Pd/SAPO 34 membrane layer were examined using field emission scanning electron microscopy (FESEM: model Leo, S430i, U. K. and Gemini, Carl ZEISS, ΣIGMA, Germany). X-ray photoelectron spectroscopy (XPS) measurements of clay–alumina support, PolyDADMAC modified support, and Pd/SAPO 34 membrane were carried out on an XPS system (PHI 5000 VersaProbe II, ULVAC-PHI, INC., USA) using a monochromatic Al Kα X-ray source (1486.6 eV). Gas permeation studies were done by a specially designed permeation cell developed in our laboratory. For permeation experiments, the membrane was mounted in a stainless steel permeation cell and sealed between two silicon O-rings. Simultaneously, the leak test was carried out before the permeation experiment of each individual gas in order to obtain the correct data. The complete description of the gas permeation measurement is given in the Supporting Information.

3. RESULTS AND DISCUSSION

A schematic representation of the membrane synthesis processes starting from bare support to nanoparticle insertion are shown in Figure 2a–f. Figure 2a shows the schematic inside view of the clay–alumina support having a negative surface charge, and subsequently, the support was modified by cationic polymer PolyDADMAC to reverse the charge of the support (Figure 2b). It is well-known that the SAPO 34 surface is rich in unsaturated −OH groups.[46] Thus, the deposition of negatively charged zeolite particles on the substrate was enhanced by attractive electrostatic forces between the zeolite seed crystal and the support surface by introducing PolyDADMAC as an intermediate linker. Then, a monolayer of nucleation seed crystals was adsorbed on the support surface (Figure 2c), followed by hydrothermal growth and formation of a homogeneous membrane layer on the support as shown in Figure 2d. Finally, presynthesized 11-mercaptoundecanoic acid capped palladium nanoparticles (MUA-Pd) were dispersed onto the membrane layer by a dip coating technique as schematically elucidated in Figure 2e. Here, the selection of PolyDADMAC as an intermediate layer was compatible because of its higher cationic charge density which can readily interact with negative surface charges. It is a synthesized linear polymer and possesses a backbone of a cyclic unit and quaternary ammonium ($-N^{+}(CH_3)_2-$) moiety found in each chain unit. As the polymer is associated with high cationic charge density, it is able to attract the negatively charged functional groups of the surface. On the basis of this concept, a probable binding mechanism of zeolite seed crystals with the support surface through the PolyDADMAC intermediate linker was depicted in Figure 2f. The electrostatic interaction occurred between the full-fledged charge center of the quaternary ammonium ($-N^{+}(CH_3)_2-$) moiety and the surface hydroxyl group of the support which formulates a smooth surface for seed layer deposition. On the other hand, an apparent electrostatic interaction also happened between the negatively charged surface hydroxyl group of zeolite seed crystals and the positively charged quaternary ammonium ($-N^{+}(CH_3)_2-$) moiety.[38] As the nitrogen atom has the positive charge on the PolyDADMAC backbone, the negatively charged SAPO 34 seed particles can easily interact with it, which facilitates the selective deposition of a uniform seed layer on the support surface.

In order to understand the interaction of PolyDADMAC with support and seed crystals, an X-ray photoelectron spectroscopy (XPS) study was carried out. Figure 3a–d describes the XPS pattern of the bare support, PolyDADMAC modified support, Pd/SAPO 34 membrane, and calcined Pd/SAPO 34 membrane, respectively. It is an effective way to investigate the interaction between the polymer and support

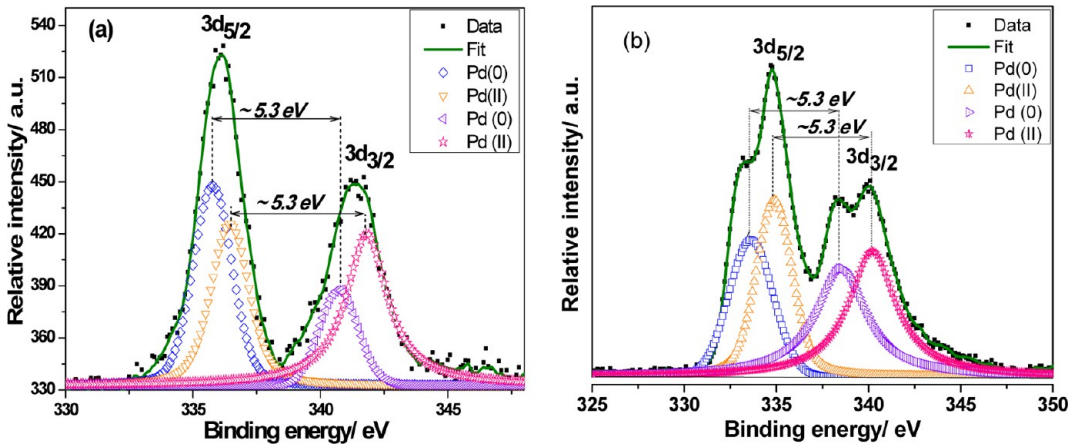

Figure 4. Fitted and deconvoluted spectra for the Pd 3d region of the Pd/SAPO 34 membrane (a) before calcinations, and (b) after calcinations. The Gaussian−Lorentzian function was used for deconvolution of the Pd 3d region.

surface. Figure 3a shows the XPS survey spectrum of the nonmodified support which reveals the presence of O 1s, Al 2p, Al 2s, Si 2p, Si 2s, and O (Auger) peaks and their related binding energies (BEs).[47] Besides those, C 1s, a small peak was found in the survey scan due to adventitious organic contamination from atmospheric exposure between sputter deposition and analysis. XPS survey spectra of the modified clay−alumina support, as displayed in Figure 3b, confirm the as proposed binding mechanism of PolyDADMAC with the support surface. The signals of Cl 2p, Cl 2s, N 1s, and C 1s appear at 199.2, 268, 400.3, and 284.7 eV in the XPS spectra, respectively, confirming the presence of the PolyDADMAC layer on the support surface.[48,49]

In addition, the other signals (O 1s, Al 2p, and Si 2p) with little intensity were obtained due to the subsequent PolyDADMAC functionalization on the support surface. The high resolution peak of the selected area (as the inset of Figure 3b) was given for better understanding. According to the literature, the most prominent peak for the N 1s XPS data shows the component at BE 402.6 eV, attributable to the $-(CH_2)_2-N^+-(CH_3)_2-$ structure, but in this case, the negative shift to lower BE (400.9 eV) was noticed and possibly due to the electrostatic interaction between the positively charged nitrogen of PolyDADMAC and the negatively charged support surface where the electron transfer occurred from the hydroxyl group (−OH) to the positively charged N^+ center of PolyDADMAC.[49] The highest intensity for C 1s at a BE of 284.7 eV was obtained due to the presence of the C−H/C−C group present in the PolyDADMAC network. Also, the XPS study was performed to ascertain the compositional information as well as the electronic state of the element present in the Pd/SAPO 34 membrane and calcined Pd/SAPO 34 membrane, respectively, as shown in Figure 3c,d. The XPS survey scan of the Pd/SAPO 34 membrane shows the O (1s and 2s), Al (2p and 2s), Si (2p and 2s), P (2s and 2p), and Pd (3d) photoelectron lines, and their corresponding BEs match well with the standard values. To obtain a better understanding of the surface chemical states of the Pd, XPS studies were performed. The XPS of the Pd 3d core level is an important method to know the electronic state of the surface region of the Pd NPs. Figure 4a,b shows the XPS deconvolution for the Pd 3d region of the uncalcined Pd/SAPO membrane and calcined Pd/SAPO 34 membrane, respectively. Figure 4a depicting the deconvoluted Pd 3d XPS curves demonstrates two sets of doublets for the Pd $3d_{3/2}$ and $3d_{5/2}$ peaks. The individual component showed that the two forms of Pd, i.e., Pd(0) and Pd(II), were present in the zeolite membrane matrix. According to the literature, the electron BEs of the Pd $3d_{5/2}$ peak for metallic Pd are in the range of 334.6−335.6 eV.[50,51]

In this case, the peak values at 335.5 and 340.8 eV denote the BEs of Pd(0) for the major spin−orbit doublet of Pd $3d_{5/2}$ and Pd $3d_{3/2}$, respectively, whereas appearance of a peak at higher values, i.e., 336.4 and 341.7 eV, attributed to its oxidation state of Pd (II). In the case of polymer/surfactant protected metal NPs, the shift to higher BEs has been related to the presence of positively charged metal atoms at the NP surface due to the interaction with the capping agent.[41,42,52,53] The same interpretation can be realized for this case also. After calcinations at inert atmosphere, the major peaks for Pd $3d_{5/2}$ appeared at 333.8 and 334.8 eV, respectively (Figure 4b).This may be due to the formation of mainly Pd (0) and a state between Pd(0) and Pd(II). This peak shifting at lower energy may be due to interaction of the Pd NPs with the zeolite matrix at the interface.[41] Thus, from the above discussion, it appeared that in the Pd/SAPO 34 membrane after thermal treatment under an inert atmosphere the Pd NPs preferably remain in a zero oxidation state.[47,54]

The transmission electron microscope (TEM) images along with selected area electron diffraction pattern (SAED) and the corresponding EDAX spectra of mercaptoundecanoic acid capped Pd NP (MUA-Pd) were provided in the Supporting Information (Figure S1). Figure 5a−d describes the TEM studies of the SAPO 34 zeolite membrane. As expected, the high resolution TEM image of the Pd/SAPO 34 membrane (Figure 5b) shows that Pd NPs were small clusters of uniform size of around ∼4−5 nm embedded in the surface of the zeolite crystals. The high-resolution TEM (HR-TEM) image illustrates the characteristic lattice fringes pattern corresponding to the Pd (111) plane. Figure 5c shows the TEM analysis of the Pd/SAPO 34 membrane after heat treatment at 550 °C under an inert atmosphere. The relatively larger Pd NPs of size ∼16.4 nm were noticed after thermal treatment. According to the literature, at higher temperature, surface melting of the nanoparticles leads to their migration on the surface and agglomeration with neighboring particles to yield large clusters.[55] After careful observation and measurement from the HR-TEM image, it shows the existence of lattice spacing equal to 0.231 nm which is close to the spacing of the (111)

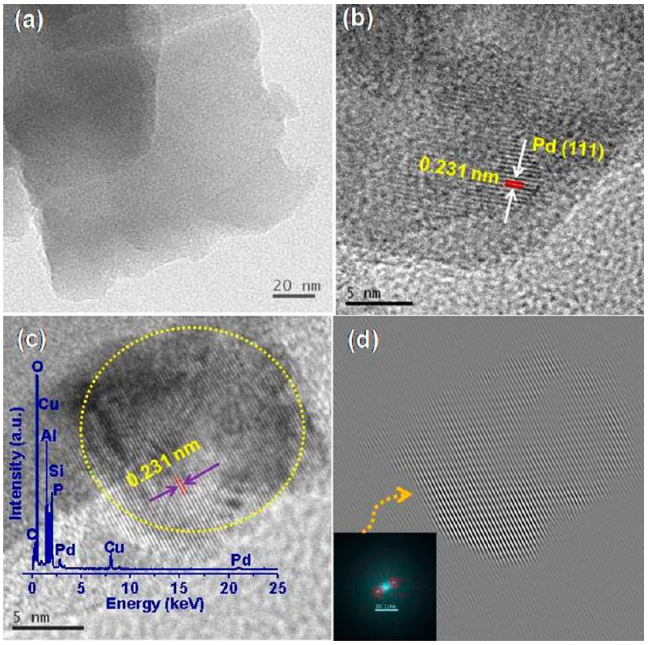

Figure 5. TEM micrograph of (a) SAPO 34 membrane layer, (b) high resolution (HRTEM) image Pd/SAPO 34 displaying the lattice fringes of the Pd nanoparticle located on the membrane layer, (c) HRTEM image of the Pd nanoparticle insertion in the membrane layer showing the crystalline fringes after the calcinations process corresponding to the Pd (111) plane (inset shows the EDS spectra of the Pd/SAPO 34 membrane), and (d) Fourier filtering images considering the Pd NPs; the inset shows the FFT pattern which clearly shows the spot corresponding to the Pd(111) lattice planes.

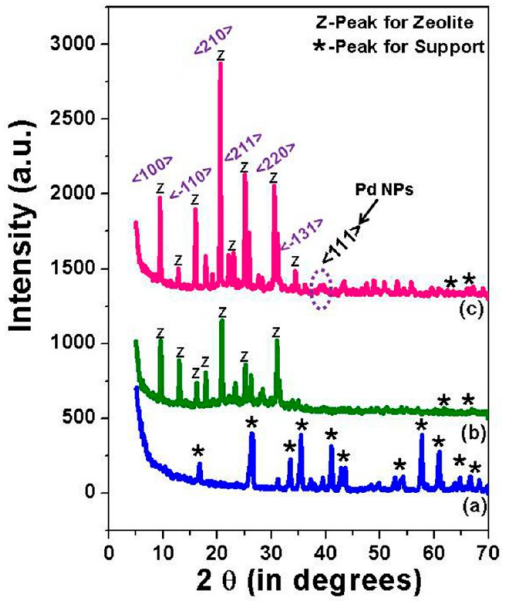

Figure 6. XRD patterns of (a) clay−alumina support, (b) the SAPO 34 membrane layer prepared on the nonmodified support, and (c) the Pd/SAPO 34 membrane layers on the modified support by the secondary growth hydrothermal technique.

planes in face centered cubic (fcc) Pd (0.223 nm) (JCPDS card no 46-1043).[56] The corresponding TEM-EDS analysis (inset of Figure 5c) confirms the presence of mainly O, Al, Si, P, and Pd. The peaks of Cu and C appear from the carbon coated Cu grid used for the TEM study. The Fourier filtering images obtained from the consequent HR-TEM image is shown in Figure 5d. In Figure 5d, the Fourier diffractogram (FFT) obtained from the nanoparticle clearly shows two spots characteristics of Pd NPs.

The formation of phase pure, highly crystalline SAPO 34 zeolite on the support surface and the existence of Pd NPs on the membrane surface were confirmed by X-ray diffraction (XRD) patterns as revealed in Figure 6a−c. Figure 6a,b depicts the XRD pattern of the bare support and the SAPO 34 membrane layer on an unmodified support, respectively. In order to compare the crystal orientation in membrane layer, XRD analysis was carried out for the membrane layer on the modified and unmodified support, respectively. The diffraction peaks obtained from the membrane layer are in agreement with those reported in the literature besides the signals from the support.[57,58] Figure 6c describes the XRD pattern of the Pd containing the SAPO 34 zeolite membrane on the modified support. From the diffraction pattern, it is clear that the intensity of the (210) peak is higher as compared to other (100), (−110), (220), (211), and (−131) peaks and proves the presence of oriented crystals in the membrane layer,[59] but the membrane prepared on the unmodified support showed the random orientation. In addition to SAPO 34 zeolite (Figure 6c), the Pd face-centered cubic phase has been identified from the Pd (111) peaks which confirms the presence of Pd NPs in the membrane layer. Compared to strong peaks that originated from SAPO 34 in the diffraction patterns, peaks associated with Pd NPs within the membrane were too weak to be observed clearly, presumably because of their small sizes or lower concentration.[60]

The result obtained from the XRD pattern explained that, during the calcination process, the presence of Pd NPs did not affect the crystal structure of the SAPO 34 zeolite, likely due to the fact that the implicated nanoparticles were too large to occupy the cavities (0.38 nm) of the framework. In general, during the heat treatment process of the as synthesized membrane, the structure-directing agents (SDA) or any other organics are removed, and as a result, nonzeolitic pores, i.e., intercrystalline gaps, defects, or cracks, are formed. Hence, it may be believed that the nonzeolitic pores were occupied by Pd NPs during the thermal treatment of the membrane and further interpretation was established by FESEM studies, EDAX analysis, and elemental mapping.

Figure 7a depicts a FESEM micrograph of the surface morphology of the Pd/SAPO 34 membrane layer prepared on the PolyDADMAC modified support. Morphology of the clay−alumina support and the seeded support has been given in the Supporting Information (Figure S2). It shows that most of the seed crystals were deposited closely and arranged homogeneously which ultimately facilitated the formation of a uniform membrane layer with an interlocking structure. No visible cracks, pinholes, or other macroscopic defects were observed on the synthesized membrane surface. Furthermore, the FESEM micrograph of the Pd/SAPO 34 membrane after thermal treatment is illustrated in Figure 7b. As the whole membrane surface was analyzed intensely by selecting a different area, the focus was to indentify the defective area and to verify the presence of nanoparticles inside it. Quick observation of the surface morphology of the membrane layer obtained from the FESEM study revealed homogeneous, interlocked dense structure, but some macroscopic defects, i.e., cracks or pinholes (indicated by the dotted circle), were observed; it was anticipated that those defects were developed during the calcination process. However, definitely the

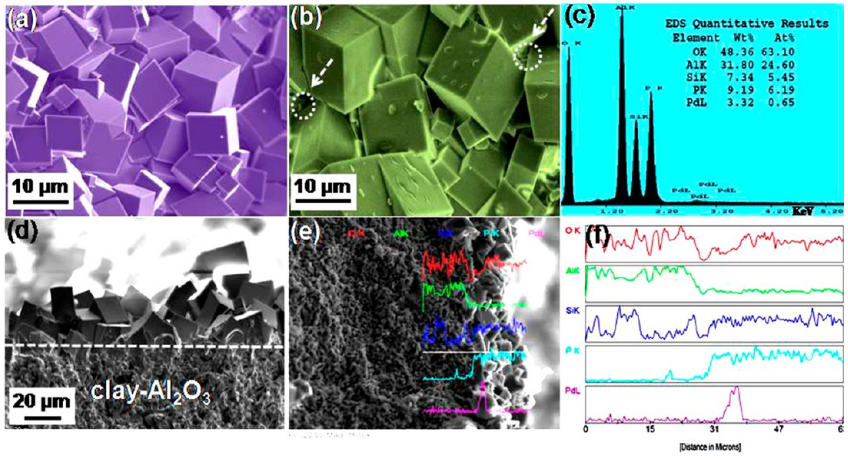

Figure 7. FESEM micrograph of the (a) synthesized Pd/SAPO 34 membrane layer, (b) calcined Pd/SAPO 34 membrane layer (the dotted circles with the arrows show the defects formed after calcinations processes), (c) corresponding EDAX spectra taken from the selected area indicated by the dotted circle (inset, table showing the quantitative analysis), (d) cross-sectional view of the Pd/SAPO 34 membrane layer, (e) cross-section with line scanning view of the Pd/SAPO 34 membrane, and (f) the corresponding spectra of O, Al, Si, P, and Pd during the elemental scan (distance in micrometers).

existence of guest Pd NPs, which occupied and plugged into the nonzeolitic pores, assisted in the development of a nearly reduced defect membrane for practical application. This elucidation was confirmed by EDAX analysis of the defective area (dotted circle) present in the membrane layer (Figure 7c). EDAX results confirm the formation of the phase pure SAPO 34 membrane along with the presence of Pd NPs which reside within the nonzeolitic pores of the membrane. The quantitative elemental analysis of the synthesized Pd/SAPO 34 membrane coating is described in the table inset in Figure 7c. Here, the quantity of Pd is comparatively lower with respect to the membrane matrix. From the above discussion, it can be concluded that, during thermal treatment, two important phenomena were carried out simultaneously: first, formation of nonzeolitic pores during the removal of structure-directing agent and, second, migration of Pd NPs which were entrapped inside the nonzeolitic pores and clogged the defects. Figure 7d describes the cross sectional view of the SAPO 34 zeolite membrane. According to the image, it can be seen that the uniform membrane layer with a thickness of about 25 μm was formed on the support surface. Figure 7e represents the cross-section view with line scanning of the Pd/SAPO 34 membrane on the modified substrate. The corresponding spectra (distance in micrometers) of O, Al, Si, P, and Pd during the elemental scan are shown in Figure 7f. During line scanning, the appearance of the phosphorus peak confirmed that the membrane layer was formed on the modified support surface only. In addition, the Pd peak was also detected during line scanning, but very interestingly, the intensity of the palladium peak was at a maximum near the interface of the membrane and support layer. It is assumed that, during thermal treatment, most of the Pd NPs penetrated rapidly deep inside the membrane layer through the intercrystalline gaps (nonzeolitic pore) and deposited at the interface. The above discussion is strongly confirmed by the EDS elemental mapping (O, Al, Si, P, and Pd) of the Pd/SAPO 34 membrane and clay−alumina cross section as illustrated in Figure 8 a−e.

It clearly shows that the O, Al, Si, and P are uniformly distributed in the membrane layer and the absence of phosphorus signals on the support confirmed that the membrane layer was developed on the modified support

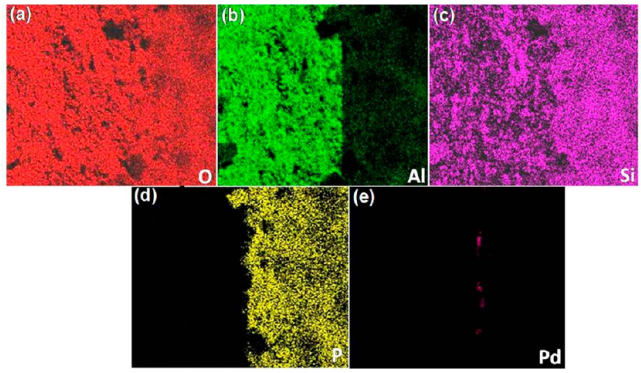

Figure 8. FESEM elemental mapping of the Pd/SAPO 34 membrane cross-section: (a) oxygen, (b) aluminum, (c) silicon, (d) phosphorus, and (d) palladium.

(Figure 8d). In addition, Figure 8e shows the deposition of a thin Pd layer at the interface of the membrane layer and finally confirms the location of the Pd NPs. The higher concentration of the Pd NPs location in the membrane-support interface after the thermal treatment process confirmed that the guest Pd NPs plays a vital role to repair the nonzeolitic pore in a suitable way. For comparison, EDAX analysis of the uncalcined Pd/SAPO 34 membrane cross section was studied as given in Figure S3 in the Supporting Information. The results showed that there is no such deposition of Pd at the membrane support interface and Pd possibly distributes on the whole membrane surface uniformly. For confirmation, FESEM elemental mapping of the Pd/SAPO 34 membrane surface was carried out and it showed that the O, Al, Si, and P are uniformly distributed within the membrane layer along with Pd. From these results, it can be explained that the migration of Pd NPs from the membrane surface to the membrane support interface through the intercrystalline gap repairs the nonzeolitic pores.

To confirm the results and repeatability of the studies, the same experiments were carried out with higher Pd loading. The results obtained are described in Figure 9a−d. Figure 9a,b shows the FESEM image of the Pd/SAPO 34 membrane cross section and the corresponding line scanning profile, respectively. The inset of Figure 9a shows the cross sectional image of

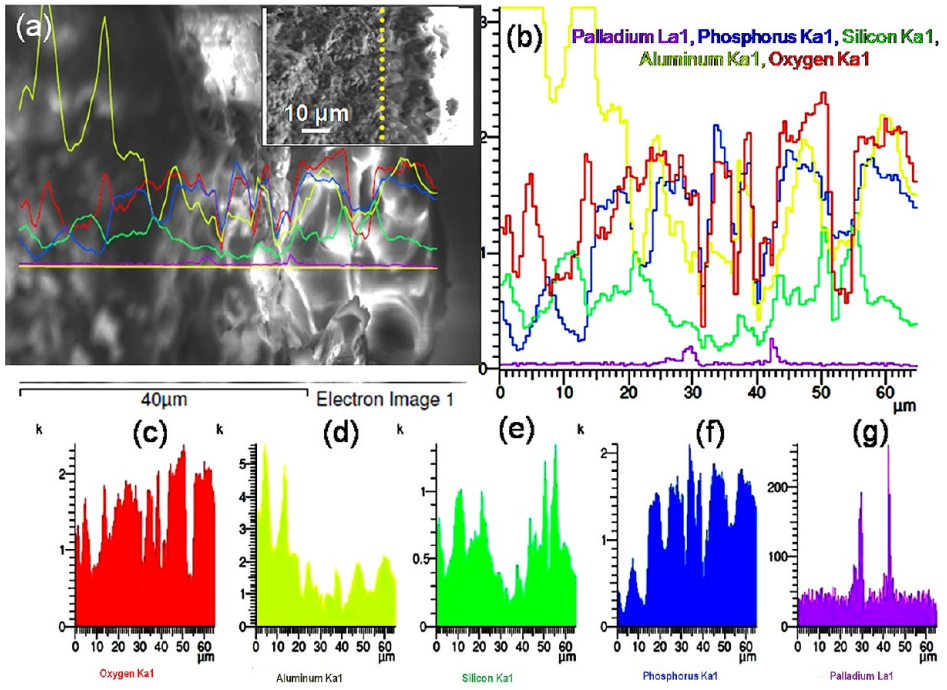

Figure 9. (a) FESEM line scanning profile of the Pd/SAPO 34 membrane cross-section (inset shows the membrane thickness), (b) corresponding spectra of O, Al, Si, P, and Pd during the elemental scan (distance in micrometers), and (c–g) spectra of individual elements.

the Pd/SAPO 34 membrane layer. The peak for the Pd was prominent at the membrane support interface. When a quick look was taken, it was observed that the Pd concentration increased at the junction, i.e., between 30 and 40 μm, where Si, Al, and P concentrations were at a minimum. According to Figure 9b, there was no Pd signal at the right side (membrane surface) or left side (support surface) of the membrane cross section.

The spectra of each element like O, Al, Si, P, and Pd are shown in Figure 9c–g, respectively. Thus, it is interesting to prove that the Pd loading with different concentrations is possible with repeatability at the interface of the Pd/SAPO 34 zeolite membrane.

This technique has the advantage that the Pd only plugs the intercrystalline gaps between zeolite crystals, i.e., nonzeolitic pores, and makes only free zeolitic pores available for gas transport. As the size of the Pd NPs was larger than the corresponding pores of the SAPO 34 zeolite (0.38 nm), they could not occupy the inside of the zeolitic pores and were occluded in the nonzeolitic pores. On the basis of these important characterization results along with the detailed explanation, it is strongly recommended that the interconnected Pd NPs facilitated the obstruction of the nonzeolitic pores and hence developed a high quality zeolite membrane for hydrogen separation. In the case of the Pd catalytic membrane, the maximum reaction has taken place at the interface. For selective H_2 permeation, at higher temperature, the dissociation and diffusion takes place at the metal–support interface. However, due to the configuration of the dense palladium membrane, permeability has been reduced to a great extent, but the porous membrane along with Pd loading in this fashion may influence the permeability and increase the reactivity of the membrane. The layer thickness of palladium may reduce the cost of the membrane. In this work, it is the most interesting phenomena noticed in the Pd loaded SAPO 34 membrane. To our knowledge, there is still no report on this kind of membrane.

Finally, in order to check the Pd/SAPO 34 membrane quality, gas permeation studies were carried out at room temperature in different feed pressures. The flow rate of different gases was controlled by the mass flow controller (MFC). Figure 10 describes the single gas permeance of

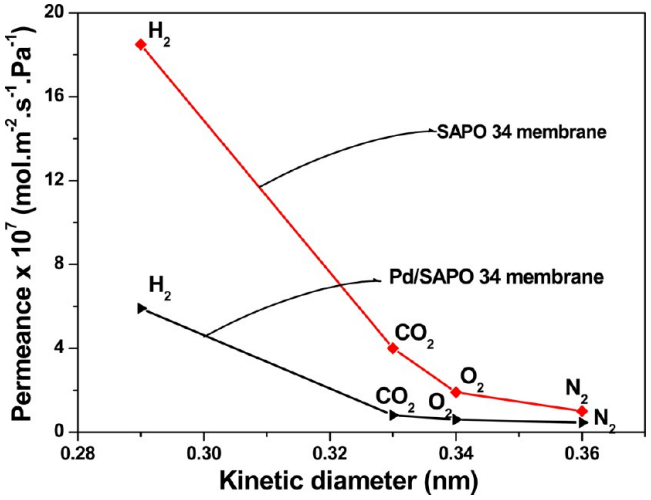

Figure 10. Single gas permeances of different gases through SAPO 34 and Pd/SAPO 34 membranes prepared on modified supports at 30 °C and 200 kPa feed pressure as a function of the gas kinetic diameter.

different gases through SAPO 34 membranes prepared on modified supports with and without Pd loading at 30 °C and 200 kPa feed pressure as a function of the gas kinetic diameter (nm). It is interesting to note that single gas permeance through the Pd/SAPO-34 membrane at room temperature changed dramatically in comparison to the SAPO 34 membrane

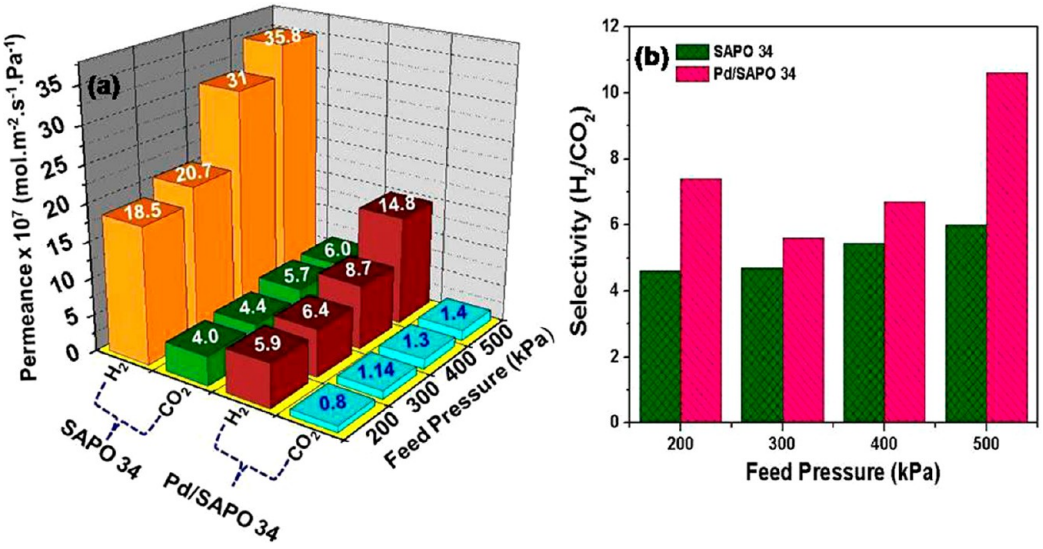

Figure 11. (a) Room temperature single gas permeation study, and (b) subsequent separation selectivity values of SAPO 34 and Pd/SAPO 34 membranes at different feed pressures (flow rate, 100 mL min^{-1}).

without Pd loading. As the kinetic diameter of H_2 (0.29 nm) is less than CO_2 (0.33 nm), O_2 (0.346 nm), and N_2 (0.364 nm), H_2 can permeate faster than other gases through the channel of the SAPO 34 zeolite having a pore size of 0.38 nm. As the kinetic diameter increased, the difference in permeability of the gases through those membranes decreased. Mostly, the significant reduction of hydrogen permeance in the case of the Pd/SAPO 34 membrane as compared to the SAPO 34 membrane indicated the drastic reduction of nonzeolitic pores. However, in the case of the SAPO 34 membrane, the higher permeance value of H_2 was obtained because of the presence of defects. From this result, it can be concluded that the nonzeolitic pores are at a minimum in the SAPO 34 membrane after Pd NPs loading.

As our work is based mainly on gas permeation studies of H_2 and CO_2, detailed permeation studies on H_2 and CO_2 at different feed pressures were carried out with the Pd/SAPO 34 membrane. Figure 11 describes the change of single gas permeability of H_2 and CO_2 and their respective separation efficiencies through the SAPO 34 and Pd/SAPO 34 zeolite membrane at different feed pressures. It shows that the rate of increase of the permeance values of CO_2 with feed pressure is less than that of H_2. At high pressure, CO_2 adsorbs more strongly on the SAPO 34 zeolite membrane surface than H_2 and the rate of desorption of CO_2 from the membrane surface also decreased as compared to H_2. Thus, with increasing pressure, the change of permeance of CO_2 was not significant. Hence, due to the preferential adsorption and diffusion of CO_2 on the SAPO 34 zeolite surface and the difference in molecular size between H_2 and CO_2, there is a difference in the permeance values through the SAPO 34 zeolite channels.

According to Figure 11a, as expected, the H_2 permeability through the Pd/SAPO 34 membrane was lower than that through the SAPO 34 zeolite membranes and the drastic reduction of the H_2 permeance value as compared to SAPO 34 indicates that nonzeolitic pores were repaired by Pd NPs. Again, in the case of Pd/SAPO 34, the CO_2 permeance values are almost equal at different feed pressures which confirms the removal of nonzeolitic pores and permeability through the Pd/zeolite membrane mainly due to the molecular sieving process which is less dependent on feed pressure. Figure 11b shows the comparative study and corresponding H_2/CO_2 selectivity values by using SAPO 34 and Pd/SAPO 34 membranes at different feed pressures. The selectivity value gradually increased with increasing feed pressure, and it was due to the higher permeance values of H_2 as compare to CO_2 at different feed pressures. The highest H_2/CO_2 selectivity value in the case of the SAPO 34 membrane was found to be 6, but in the case of the Pd/SAPO 34 membrane, it was 10.6. The enhancement of the separation performance is probably attributed due to the reduction of nonzeolitic pores in the Pd/SAPO membrane and the longer effective diffusion path through the whole membrane thickness. The synthesized membrane shows higher hydrogen permeation results, because of the membrane layer orientation. As the membrane structure was associated with the maximum number of oriented crystals, the pores were more aligned. As a result, the resistance of the gas transport through the aligned channel was less, and accordingly, membrane resistance decreased and permeation adequacy of H_2 through the membrane was enhanced.

The real performance of the membrane for hydrogen gas separation from a mixture can be evaluated from their mixture gas separation studies. Figure 12 describes the comparison of permeance of H_2 and CO_2 in a binary gas mixture (H_2/CO_2 = 55:45) as well as single gas permeation. In the case of a single gas, the permeance, of both H_2 and CO_2, remains almost constant with increasing feed pressure. It indicates that the nonzeolitic pores in the Pd/SAPO 34 membrane have been removed appreciably, but in case of a mixture gas, the permeance of H_2 is reduced drastically compared to CO_2 with increasing feed pressure. This phenomenon can be explained by an adsorption−diffusion mechanism. With increasing feed pressure, CO_2 adsorbed preferentially compared to H_2 because of its stronger electrostatic quadruple moment and the permeability remained almost the same. On the other hand, in the case of H_2 permeability, due to preferential occupancy by CO_2, the permeability of H_2 through the zeolite pores was hindered and reduced; as a result, the H_2/CO_2 mixture separation factor was reduced with respect to different feed pressures.

The highest mixture gas separation factor for the Pd/SAPO 34 membrane was achieved at 20.8. However, the mixture

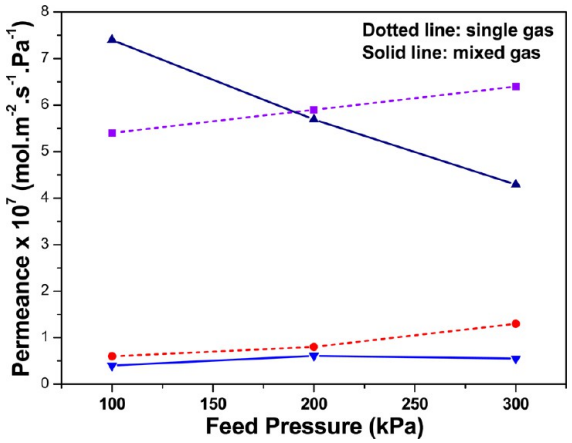

Figure 12. Permeance of H_2 and CO_2 for a single gas (dotted line) and a mixture gas (solid line) (H_2/CO_2 55:45) at 30 °C as a function of feed pressure for the Pd/SAPO 34 membrane (flow rate, 100 mL min^{-1}).

separation factor in the case of the SAPO 34 membrane was 6.2. The change of the separation factor of H_2/CO_2 gas mixture with a different membrane is described in Figure 13. It is clear

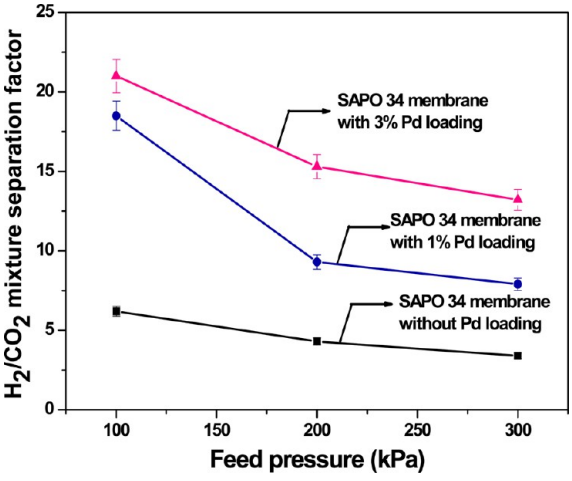

Figure 13. Room temperature H_2/CO_2 (55:45) mixture separation factor as a function of different feed pressures for the SAPO 34 membrane and the SAPO 34 membrane with different Pd loadings (flow rate, 100 mL min^{-1}). Error bars signify variance in GC injection measurements.

from the figure that the separation factor increases with increasing Pd NP loading in the SAPO 34 membrane. The higher NP loading removed and repaired more nonzeolitic pores, and as a result, the H_2/CO_2 separation factor increased accordingly. Both values, i.e., hydrogen permeation[33,34,60] (as shown in Table 1) and separation factors, were higher than the literature values.[15,16,45] Combining all these aspects, it is concluded that the separation selectivity of the SAPO membranes increases tremendously after insertion of the Pd NPs which can reduce the nonzeolitic pores to a large extent and improve the membrane quality for hydrogen gas separation.

4. CONCLUSIONS

The present paper highlighted how the nonzeolitic pores of the synthesized membrane can be repaired by the insertion of palladium nanoparticles in the membrane matrix which shows higher H_2/CO_2 separation results as compared to the synthesized SAPO 34 membrane. Orientation and drastic reduction of nonzeolitic pores in the membrane layer may enhance the membrane quality for gas separation application. It has been investigated and found that the intermediate layer plays an important role and offers a convenient process for seed layer deposition and an important step to minimize the nonzeolitic pores in the earlier stages of membrane fabrication. In addition to experimental evidence, the permeation results of hydrogen gas at different feed pressures for the SAPO 34 membrane and the Pd/SAPO 34 membrane demonstrated the drastic reduction of nonzeolitic pores in the membrane layer. The noticeable improvement in the H_2/CO_2 mixture separation factor from the SAPO 34 membrane to Pd/SAPO 34 finally satisfied the objective of synthesizing an almost defect free membrane. The H_2/CO_2 mixture separation factor was increased up to 20.8 at room temperature, but in case of the SAPO 34 membrane without Pd loading, the separation factor was 6.2. For the first time, we have synthesized the Pd loaded high quality SAPO 34 membrane in an easy and simple route. Moreover, the selection of a natively developed low-cost support ultimately reduced the membrane cost. Combining all these important aspects along with the interesting experimental evidence, the synthesized membrane is highly qualified for hydrogen gas separation application. As the membrane is not completely defect free, still, improvement is needed to enhance the separation performance. Apart from gas separation application, the palladium nanoparticle loaded membrane may be implemented for various applications especially for high temperature application. The most interesting part of this work is the deposition of Pd nanoparticles in the form of a thin layer at the support membrane interface, which may be useful for synthesizing metal loaded catalytic membranes in the future.

■ ASSOCIATED CONTENT

Supporting Information

TEM images along with the SAED pattern and the corresponding EDAX spectra of 11-mercaptoundecanoic acid capped palladium nanoparticles (MUA-Pd), morphology of the clay−alumina support and the SAPO 34 seeded support, and EDAX analysis of the uncalcined Pd/SAPO 34 membrane cross

Table 1. Comparison of Hydrogen Permeance of Pd/SAPO 34 Membrane with Literature Values

membrane	support	temp. (K)	method to repair nonzeolitic pores	deposition technique	remark	H_2 permeances ($mol \cdot m^{-2} \cdot s^{-1} \cdot Pa^{-1}$)	ref.
Pd/zeolite A	α-Al_2O_3	473	impregnation of Pd salt	CVD	high cost	2.65×10^{-7}	33
Pd/Si-MFI	α-Al_2O_3	303	deposition of Pd NPs	CFT	high cost		34
C/SAPO 34	α-Al_2O_3	298	thin carbon coating	dip-coating	easy	10×10^{-8}	61
Pd/SAPO 34	low-cost clay-Al_2O_3	303	deposition of Pd NPs	dip-coating	cost-effective and easy	14.8×10^{-7}	this study

section. This material is available free of charge via the Internet at http://pubs.acs.org.

AUTHOR INFORMATION

Corresponding Author

*E-mail: dasnandini@cgcri.res.in. Tel.: +91 33 2483 8082. Fax: +91 033 2473 0957.

Notes

The authors declare no competing financial interest.

ACKNOWLEDGMENTS

Financial support from the CSIR, India, Government of India, under the project ESC 0104 is thankfully acknowledged. The authors would like to thank Mr. Kamal Dasgupta, Director, CGCRI for his kind permission to publish the research work. Dr. Manjay Sreemany and Ashok K. Mondal are thanked for their support in electron microscopy.

REFERENCES

(1) Lubitz, W.; Tumas, W. Hydrogen: An Overview. *Chem. Rev.* **2007**, *107*, 3900−3903.

(2) Gunardson, H. *Synthesis Gas Manufacture, Industrial Gases in Petrochemical Processing*; Marcel Dekker, Inc.: New York, 1998; Chapter 2, pp 41−80.

(3) Ozin, G. A.; Kuperman, A.; Stein, A. Advanced Zeolite Materials Science. *Adv. Mater.* **1989**, *1*, 69−86.

(4) Tavolaro, A.; Drioli, E. Zeolite Membranes. *Adv. Mater.* **1999**, *11*, 975−996.

(5) Lovallo, M. C.; Tsapatsis, M. Preferentially Oriented Submicron Silicalite Membranes. *AIChE J.* **1996**, *42*, 3020−3029.

(6) Huang, A.; Liang, F.; Steinbach, F.; Caro, J. Preparation and Separation Properties of LTA Membranes by Using 3-Aminopropyltriethoxysilane as Covalent Linker. *J. Membr. Sci.* **2010**, *350*, 5−9.

(7) Himeno, S.; Tomita, T.; Suzuki, K.; Nakayama, K.; Yajima, K.; Yoshida, S. Synthesis and Permeation Properties of a DDR-Type Zeolite Membrane for Separation of CO_2/CH_4 Gaseous Mixtures. *Ind. Eng. Chem. Res.* **2007**, *46*, 6989−6997.

(8) Yu, M.; Funke, H. H.; Noble, R. D.; Falconer, J. L. H_2 Separation Using Defect-Free, Inorganic Composite Membranes. *J. Am. Chem. Soc.* **2011**, *133*, 1748−1750.

(9) Mintova, S.; Mo, S.; Bein, T. Nanosized $AlPO_4$-5 Molecular Sieves and Ultrathin Films Prepared by Microwave Synthesis. *Chem. Mater.* **1998**, *10*, 4030−4036.

(10) Nikolakis, V.; Xomeritakis, G.; Abibi, A.; Dickson, M.; Tsapatsis, M.; Vlachos, D. G. Growth of a Faujasite-Type Zeolite Membrane and Its Application in the Separation of Saturated/Unsaturated Hydrocarbon Mixtures. *J. Membr. Sci.* **2001**, *184*, 209−219.

(11) Li, S.; Falconer, J. L.; Noble, R. D. SAPO-34 Membranes for CO_2/CH_4 Separation. *J. Membr. Sci.* **2004**, *241*, 121−135.

(12) Djieugoue, M. A.; Prakash, A. M.; Kevan, L. Catalytic Study of Methanol-to-Olefins Conversion in Four Small-Pore Silicoaluminophosphate Molecular Sieves: Influence of the Structural Type, Nickel Incorporation, Nickel Location, and Nickel Concentration. *J. Phys. Chem. B* **2000**, *104*, 6452−6461.

(13) Oikawa, H.; Shibata, Y.; Inazu, K.; Iwase, Y.; Murai, K.; Hyodo, S.; Kobayashi, G.; Baba, T. Highly Selective Conversion of Ethene to Propene over SAPO-34 as a Solid Acid Catalyst. *Appl. Catal., A* **2006**, *312*, 181−185.

(14) Shang, J.; Li, G.; Singh, R.; Gu, Q.; Nairn, K. M.; Bastow, T. J.; Medhekar, N.; Doherty, C. M.; Hill, A. J.; Liu, J. Z.; Webley, P. A. Discriminative Separation of Gases by a "Molecular Trapdoor" Mechanism in Chabazite Zeolites. *J. Am. Chem. Soc.* **2012**, *134*, 19246−19253.

(15) Poshusta, J. C.; Tuan, V. A.; Falconer, J. L.; Noble, R. D. Synthesis and Permeation Properties of SAPO-34 Tubular Membranes. *Ind. Eng. Chem. Res.* **1998**, *37*, 3924−3929.

(16) Poshusta, J. C.; Tuan, V. A.; Pape, E. A.; Falconer, J. L.; Noble, R. D. Separation of Light Gas Mixtures Using SAPO-34 Membranes. *AIChE J.* **2000**, *46*, 779−789.

(17) Hong, M.; Li, S.; Falconer, J. L.; Noble, R. D. Hydrogen Purification Using a SAPO-34 Membrane. *J. Membr. Sci.* **2008**, *307*, 277−283.

(18) Venna, S. R.; Carreon, M. A. Amino-Functionalized SAPO-34 Membranes for CO_2/CH_4 and CO_2/N_2 Separation. *Langmuir* **2011**, *27*, 2888−2894.

(19) Li, S.; Fan, C. Q. High-Flux SAPO-34 Membrane for CO_2/N_2 Separation. *Ind. Eng. Chem. Res.* **2010**, *49*, 4399−4404.

(20) Das, J. K.; Das, N.; Bandyopadhyay, S. Highly Oriented Improved SAPO 34 Membrane on Low Cost Support for Hydrogen Gas Separation. *J. Mater. Chem. A* **2013**, *1*, 4966−4973.

(21) Caro, J.; Noack, M.; Kolsch, P.; Schafer, R. Zeolite Membranes−State of Their Development and Perspective. *Microporous Mesoporous Mater.* **2000**, *38*, 3−24.

(22) Baker, R. W. Future Directions of Membrane Gas Separation Technology. *Ind. Eng. Chem. Res.* **2002**, *41*, 1393−1411.

(23) Zhang, B.; Wang, C.; Lang, L.; Cui, R.; Liu, X. Selective Defect-Patching of Zeolite Membranes Using Chemical Liquid Deposition at Organic/Aqueous Interfaces. *Adv. Funct. Mater.* **2008**, *18*, 3434−3443.

(24) Choi, J.; Jeong, H. K.; Snyder, M. A.; Stoeger, J. A.; Masel, R. I.; Tsapatsis, M. Grain Boundary Defect Elimination in a Zeolite Membrane by Rapid Thermal Processing. *Science* **2009**, *325*, 590−593.

(25) Yan, Y. S.; Davis, M. E.; Gavalas, G. R. Preparation of Highly Selective Zeolite ZSM-5 Membranes by a Post-Synthetic Coking Treatment. *J. Membr. Sci.* **1997**, *123*, 95−103.

(26) Hirota, Y.; Watanabe, K.; Uchida, Y.; Egashira, Y.; Yoshida, K.; Sasaki, Y.; Nishiyama, N. Coke Deposition in the SAPO-34 Membranes for Examining the Effects of Zeolitic and Non-Zeolitic Pathways on the Permeation and Separation Properties in Gas and Vapor Permeations. *J. Membr. Sci.* **2012**, *415*, 176−180.

(27) Xomeritakis, G.; Lai, Z. P.; Tsapatsis, M. Separation of Xylene Isomer Vapors with Oriented MFI Membranes Made by Seeded Growth. *Ind. Eng. Chem. Res.* **2001**, *40*, 544−552.

(28) Nair, S.; Lai, Z. P.; Nikolakis, V.; Xomeritakis, G.; Bonilla, G.; Tsapatsis, M. Separation of Close-Boiling Hydrocarbon Mixtures by MFI and FAU Membranes Made by Secondary Growth. *Microporous Mesoporous Mater.* **2001**, *48*, 219−228.

(29) Matsuda, H.; Yanagishita, H.; Negishi, H.; Kitamoto, D.; Ikegami, T.; Haraya, K.; Nakane, T.; Idemoto, Y.; Koura, N.; Sano, T. Improvement of Ethanol Selectivity of Silicalite Membrane in Pervaporation by Silicone Rubber Coating. *J. Membr. Sci.* **2002**, *210*, 433−437.

(30) Nomura, M.; Yamaguchi, T.; Nakao, S. Silicalite Membranes Modified by Counterdiffusion CVD Technique. *Ind. Eng. Chem. Res.* **1997**, *36*, 4217−4223.

(31) McHenry, J. A.; Deckman, H. W.; Corcoran, E. W., Jr.; Lai, W. F.; Witzke H. *Membrane Reparation and Pore Size Reduction Using Interfacial Ozone Assisted Chemical Vapor Deposition* (Exxon Research & Engineering Company); U.S. Patent 5,672,388, 1997.

(32) Anthonis, M. H.; Bons, A. J.; Czarnetzki, L. R.; DeGijnst, W. G. J.; Mortier, W. J.; Van Oorschot, C. W. M. *Molecular Sieves and Processes for Their Manufacture* (Exxon Chemical Patents Inc.); U.S. Patent 6,074,457, 2000.

(33) Morón, F.; Pina, M. P.; Urriolabeitia, E.; Menéndez, M.; Santamaría, J. Preparation and Characterization of Pd-Zeolite Composite Membranes for Hydrogen Separation. *Desalination* **2002**, *147*, 425−431.

(34) Liu, X.; Liu, W.; Li, J.; Zhang, Y.; Lang, L.; Ma, L.; Zhang, B. Reactive Deposition of Palladium Nanoparticles onto Zeolite Membranes in Supercritical CO_2. *Ind. Eng. Chem. Res.* **2010**, *49*, 8826−8831.

(35) Algieri, C.; Bernardo, P.; Barbieri, G.; Drioli, E. A Novel Seeding Procedure for Preparing Tubular NaY Zeolite Membranes. *Microporous Mesoporous Mater.* **2009**, *119*, 129−136.

(36) Oonkhanond, B.; Mullins, M. E. The Preparation and Analysis of Zeolite ZSM-5 Membranes on Porous Alumina Supports. *J. Membr. Sci.* **2001**, *194*, 3−13.
(37) Wang, X.; Zhang, B.; Liu, X.; Lin, Y. S. Synthesis of *b*-Oriented TS-1 Films on Chitosan-Modified α-Al_2O_3Substrates. *Adv. Mater.* **2006**, *18*, 3261−3265.
(38) Lee, G. S.; Lee, Y. J.; Yoon, K. B. Layer-by-Layer Assembly of Zeolite Crystals on Glass with Polyelectrolytes as Ionic Linkers. *J. Am. Chem. Soc.* **2001**, *123*, 9769−9779.
(39) Hedlund, J.; Schoeman, B.; Sterte, J. Ultrathin Oriented Zeolite LTA Films. *Chem. Commun.* **1997**, 1193−1194.
(40) Kuzniatsova, T. A.; Mottern, M. L.; Chiu, W. V.; Kim, Y.; Dutta, P. K.; Verweij, H. Synthesis of Thin, Oriented Zeolite A Membranes on a Macroporous Support. *Adv. Funct. Mater.* **2008**, *18*, 952−958.
(41) Miguel-Garcia, I.; Berenguer-Murcia, A.; Cazorla-Amoros, D. Preferential Oxidation of CO Catalyzed by Supported Polymer-Protected Palladium-Based Nanoparticles. *Appl. Catal., B* **2010**, *98*, 161−170.
(42) Navin, J. K.; Grass, M. E.; Somorjai, G. A.; Marsh, A. L. Characterization of Colloidal Platinum Nanoparticles by MALDI-TOF Mass Spectrometry. *Anal. Chem.* **2009**, *81*, 6295−6299.
(43) Cargnello, M.; Wieder, N. L.; Canton, P.; Montini, T.; Giambastiani, G.; Benedetti, A.; Gorte, R. J.; Fornasiero, P. A Versatile Approach to the Synthesis of Functionalized Thiol-Protected Palladium Nanoparticles. *Chem. Mater.* **2011**, *23*, 3961−3969.
(44) Laursen, A. B.; Højholt, K. T.; Lundegaard, L. F.; Simonsen, S. B.; Helveg, S.; Schuth, F.; Paul, M.; Grunwaldt, J.; Kegnæs, S.; Christensen, C. H.; Egeblad, K. Substrate Size-Selective Catalysis with Zeolite-Encapsulated Gold Nanoparticles. *Angew. Chem.* **2010**, *49*, 3504−3507.
(45) Das, J. K.; Das, N.; Bandyopadhyay, S. Highly Selective SAPO 34 Membrane on Surface Modified Clay−Alumina Tubular Support for H_2/CO_2 Separation. *Int. J. Hydrogen Energy* **2012**, *37*, 10354−10364.
(46) Jeanvoine, Y.; Angyan, J. G.; Kresse, G.; Hafner, J. Brønsted Acid Sites in HSAPO-34 and Chabazite: An ab Initio Structural Study. *J. Phys. Chem. B* **1998**, *102*, 5573−5580.
(47) Chen, R.; Jiang, Y.; Xing, W.; Jin, W. Fabrication and Catalytic Properties of Palladium Nanoparticles Deposited on a Silanized Asymmetric Ceramic Support. *Ind. Eng. Chem. Res.* **2011**, *50*, 4405−4411.
(48) Nakayama, M.; Tagashira, H. Electrodeposition of Layered Manganese Oxide Nanocomposites Intercalated with Strong and Weak Polyelectrolytes. *Langmuir* **2006**, *22*, 3864−3869.
(49) Wang, S.; Yu, D.; Dai, L.; Chang, D. W.; Baek, J. B. Polyelectrolyte-Functionalized Graphene as Metal-Free Electrocatalysts for Oxygen Reduction. *ACS Nano* **2011**, *8*, 6202−6209.
(50) Witonska, I. A.; Walock, M. J.; Binczarski, M.; Lesiak, M.; Stanishevsky, A. V.; Karski, S. Pd−Fe/SiO_2 and Pd−Fe/Al_2O_3 Catalysts for Selective Hydrodechlorination of 2,4-Dichlorophenol into Phenol. *J. Mol. Catal. A: Chem.* **2014**, *393*, 248−256.
(51) Sharma, S.; Kim, B.; Lee, D. Water-Soluble Pd Nanoparticles Capped with Glutathione: Synthesis, Characterization, and Magnetic Properties. *Langmuir* **2012**, *28*, 15958−15965.
(52) Borodko, Y.; Humphrey, S. M.; Tilley, T. D.; Frei, H.; Somorjai, G. A. Charge-Transfer Interaction of Poly(vinylpyrrolidone) with Platinum and Rhodium Nanoparticles. *J. Phys. Chem. C* **2007**, *111*, 6288−6295.
(53) Borodko, Y.; Habas, S. E.; Koebel, M.; Yang, P.; Frei, H.; Somorjai, G. A. Probing the Interaction of Poly(vinylpyrrolidone) with Platinum Nanocrystals by UV-Raman and FTIR. *J. Phys. Chem. B* **2006**, *110*, 23052−23059.
(54) Kidambi, S.; Bruening, M. L. Multilayered Polyelectrolyte Films Containing Palladium Nanoparticles: Synthesis, Characterization, and Application in Selective Hydrogenation. *Chem. Mater.* **2005**, *17*, 301−307.
(55) Park, J. C.; Song, H. Metal@Silica Yolk−Shell Nanostructures as Versatile Bifunctional Nanocatalysts. *Nano Res.* **2011**, *4*, 33−49.
(56) Liu, Y.; Wang, C.; Wei, Y.; Zhu, L.; Li, D.; Jiang, J. S.; Markovic, N. M.; Stamenkovic, V. R.; Sun, S. Surfactant-Induced Postsynthetic Modulation of Pd Nanoparticle Crystallinity. *Nano Lett.* **2011**, *11*, 1614−1617.
(57) Dumitriu, E.; Azzouz, A.; Hulea, V.; Lutic, D.; Kessler, H. Synthesis, Characterization and Catalytic Activity of SAPO-34 Obtained with Piperidine as Templating Agent. *Microporous Mater.* **1997**, *10*, 1−12.
(58) Tan, J.; Liu, Z.; Bao, X.; Liu, X.; Han, X.; He, C.; Zhai, R. Crystallization and Si Incorporation Mechanisms of SAPO-34. *Microporous Mesoporous Mater.* **2002**, *53*, 97−108.
(59) Huang, A.; Caro, J. Cationic Polymer Used to Capture Zeolite Precursor Particles for the Facile Synthesis of Oriented Zeolite LTA Molecular Sieve Membrane. *Chem. Mater.* **2010**, *22*, 4353−4355.
(60) Lu, G.; Li, S.; Guo, Z.; Farha, O. K.; Hauser, B. G.; Qi, X.; Wang, Y.; Wang, X.; Han, S.; Liu, X.; DuChene, J. S.; Zhang, H.; Zhang, Q.; Chen, X.; Ma, J.; Loo, S. C. J.; Wei, W. D.; Yang, Y.; Hupp, J. T.; Huo, F. Imparting Functionality to a Metal−Organic Framework Material by Controlled Nanoparticle Encapsulation. *Nat. Chem.* **2012**, *4*, 310−316.
(61) Li, G.; Yang, J.; Wang, J.; Xiao, W.; Zhou, L.; Zhang, Y.; Lu, J.; Yin, D. Thin Carbon/SAPO-34 Microporous Composite Membranes for Gas Separation. *J. Membr. Sci.* **2011**, *374*, 83−92.